Rapid Calculation of the Green's Function in a Rectangular Enclosure With Application to Conductor Loaded Cavity Resonators

Amir Borji, *Member, IEEE,* and Safieddin Safavi-Naeini, *Member, IEEE*

***Abstract*—A new technique for rapid calculation of the Green's functions in a rectangular cavity is presented. The method is based on a best polynomial approximation in three dimensions, which is implemented through a fast cosine transform. Generating the required samples for polynomial modeling is greatly accelerated through Ewald summation technique. To validate the efficiency of the resulting Chebyshev series for the potential Green's functions, a surface integral-equation (SIE) formulation is used to compute the resonant frequency of conductor loaded cavity resonators. The new scheme is proved to be considerably faster than Ewald transform in filling the method of moments (MoM) matrix. A SIE with the MoM can now be efficiently used for electromagnetic analysis and optimization of conductor or dielectric loaded resonators and filters with rectangular enclosures.**

***Index Terms*—Chebyshev polynomial approximation, Green's function, rectangular cavity, surface integral equation (SIE).**

I. Introduction

SURFACE integral-equation (SIE) technique with the method of moments (MoM) is a versatile and efficient method for electromagnetic analysis of arbitrarily shaped dielectric and metallic objects, but the slow convergence of the relevant Green's functions inside a rectangular enclosure makes it very difficult, if not impossible, for this method to be applied for the analysis of shielded objects. Different convergence acceleration schemes have been utilized in effort to apply an SIE MoM for shielded structures. These applications have been mostly restricted to electromagnetic compatibility (EMC)/electromagnetic interference (EMI) studies including wire antennas and septums inside rectangular enclosures [1]. In [2]–[4], an asymptotic extraction method was used to calculate the field coupling to cavities or rectangular waveguides via coaxial probes. Usually in those cases, only one or two components of the Green's functions are required, and since the number of unknowns is relatively small, conventional convergence acceleration techniques lead to a fairly efficient solution. The Ewald summation technique has proven to be a very effective tool for rapid calculation of potential Green's functions in periodic structures, as well as cavities and waveguides [5]–[8]. Theoretically, this method yields the highest possible overall convergence rate among series acceleration techniques for rectangular cavity Green's function, but has only been used by few researchers [1].

In [9], the Ewald transform was used to accelerate the convergence of the quasi-static part of the Green's function in a boundary integral formulation to analyze waveguide filters. Using SIE MoM for full-wave analysis of metallic or dielectric loaded cavity resonators and filters, though appealing at first sight, has not been implemented successfully so far due to computational complexity of the pertinent Green's functions, rendering the method to be very inefficient compared to the finite-element or mode-matching techniques. It will be shown in this paper that, even after using the Ewald method, it will not be feasible to use the integral-equation technique for full-wave analysis or direct optimization of these structures.

In this paper, a new scheme for very fast computation of the Green's functions in a rectangular box is introduced, which is based on a Chebyshev polynomial approximation of the vector and scalar potentials. This polynomial modeling process needs to be repeated for each frequency. Using a fast cosine transform (FCT) for polynomial approximation combined with the Ewald acceleration method for generating the required samples makes this process extremely fast so that its computational overhead is negligible. During the Chebyshev approximation process, the source is located at the origin, and the singularity of the function is extracted. An interesting feature of this approach is that, after evaluating the polynomial model eight times, corresponding to locations of the source and its seven immediate images, *all* components of the electric and magnetic vector and scalar potentials are calculated *simultaneously* for an arbitrary source location without further call to the polynomial model.

For validation and comparison purposes, both the Ewald method and new polynomial model are used in an SIE–MoM formulation in order to find the resonant frequency of some commonly used conductor loaded cavity resonators. This includes a cavity loaded with a metallic disk and a combline cavity resonator. Our new approach reduces the matrix filling time in a full-wave SIE–MoM solution by an average factor of 30 compared to Ewald transform without loss of accuracy. With a drastic reduction in computational time while maintaining high accuracy, it is now feasible to use the integral-equation technique and MoM for direct optimization of structures made of dielectric or metallic objects inside rectangular cavities.

Manuscript received September 28, 2003; revised January 6, 2004.

The authors are with the Department of Electrical and Computer Engineering, University of Waterloo, Waterloo, ON, Canada N2L 3G1 (e-mail: amir@maxwell.uwaterloo.ca; safavi@maxwell.uwaterloo.ca).

Digital Object Identifier 10.1109/TMTT.2004.830488

II. Theory

In a rectangular cavity uniformly filled with a homogeneous material with a dielectric constant of ϵ_r, there are three components for each of the electric $(\vec{F})$ and magnetic $(\vec{A})$ vector potential Green's functions

$$\bar{\bar{G}}_{A,F} = G_{A,F}^{xx}\hat{x}\hat{x} + G_{A,F}^{yy}\hat{y}\hat{y} + G_{A,F}^{zz}\hat{z}\hat{z} \tag{1}$$

as well as two scalar potentials $G_q^{e,m}$ corresponding to electric and magnetic sources. In the following sections, G_A^{xx} is chosen for demonstration of the method. Other components are treated in an identical manner.

A. Image Series Representation

Consider an infinitesimal $\hat{x}$-directed electric dipole located inside a homogenous rectangular cavity. Fig. 1 shows a basic cell of the source and its immediate images due to the adjacent walls of the cavity. The complete set of images is obtained by repeating the basic cell with a period of $2a \times 2b \times 2c$ in space where a, b, and c are the dimensions of the cavity along the $\hat{x}$-, $\hat{y}$-, and $\hat{z}$-directions, respectively. The magnetic vector potential for this distribution of sources is G_A^{xx} as follows:

$$\frac{G_A^{xx}}{\mu_0} = \frac{1}{4\pi}\sum_{m=-\infty}^{+\infty}\sum_{n=-\infty}^{+\infty}\sum_{p=-\infty}^{+\infty}\sum_{i=0}^{7} A_i \frac{e^{-jkR_{i,mnp}}}{R_{i,mnp}} \tag{2a}$$

$$R_{i,mnp} = \sqrt{(X_i - 2ma)^2 + (Y_i - 2nb)^2 + (Z_i - 2pc)^2} \tag{2b}$$

$k = (2\pi)/(\lambda_0)\sqrt{\epsilon_r}$ is the wavenumber inside the box and A_i is $+1$ or -1 corresponding to the relative orientation of the source and its images in the basic cell. In Fig. 1, the orientation of each dipole is represented by a $+/-$ sign from which the value of A_i is obtained. It can be shown that $X_i = |x - x_i'|$, $Y_i = |y - y_i'|$, and $Z_i = |z - z_i'|$, where (x, y, z) is the location of the observation point and $(x_i', y_i\prime, z_i')$ is the position of the ith dipole in the basic cell of images shown in Fig. 1. Components of the potential Green's functions *only* differ in their corresponding A_i coefficients, i.e., the only difference among them is the orientation of basic images of the source. Equation (2a) can be written in the following form:

$$\begin{aligned}\frac{G_A^{xx}}{\mu_0} = {} & G\big(|x-x'|, |y-y'|, |z-z'|\big) \\ & - G\big(|x-x'|, |y-y'|, z+z'\big) \\ & - G\big(|x-x'|, y+y', |z-z'|\big) \\ & + G\big(|x-x'|, y+y', z+z'\big) \\ & + G\big(x+x', |y-y'|, |z-z'|\big) \\ & - G\big(x+x', |y-y'|, z+z'\big) \\ & - G\big(x+x', y+y', |z-z'|\big) \\ & + G\big(x+x', y+y', z+z'\big)\end{aligned} \tag{3}$$

in which

$$G(u,v,w) \triangleq \frac{1}{4\pi}\sum_{m=-\infty}^{+\infty}\sum_{n=-\infty}^{+\infty}\sum_{p=-\infty}^{+\infty}\frac{e^{-jkR_{mnp}}}{R_{mnp}} \tag{4a}$$

$$R_{mnp} = \sqrt{(u-2ma)^2 + (v-2nb)^2 + (w-2pc)^2}. \tag{4b}$$

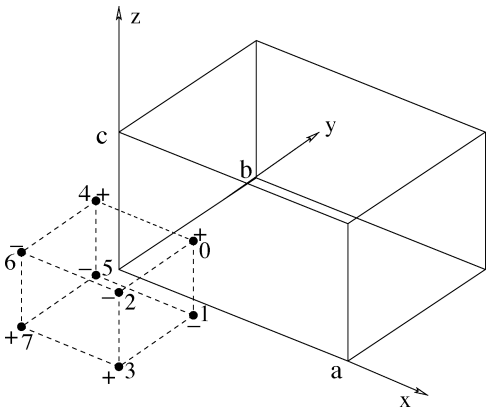

Fig. 1. Basic cell of images. This cell is repeated with a period of $2a \times 2b \times 2c$.

It can be shown that $G(u, v, w)$ is an even function of u, v, and w. It is also a periodic function with a spatial period of ($2a$, $2b$, $2c$) and is evenly symmetric with respect to $u = a$, $v = b$, and $w = c$ planes as follows:

$$G(u,v,w) = G(\pm u, \pm v, \pm w) = G(2a \pm u, 2b \pm v, 2c \pm w). \tag{5}$$

In the proposed scheme, $G(u, v, w)$ is approximated by a finite series of Chebyshev polynomials. The main advantage of writing G_A^{xx} in the form of (3) is that, instead of a six variable function, as in (2a), one has to deal with a three-variable function, which is more appropriate for modeling purposes. Another major advantage of the above approach is that, after an appropriate model for $G(u, v, w)$ is obtained, all the components of vector and scalar potentials are calculated through an equation identical to (3) with the only difference being the $+/-$ signs, i.e., the eight terms in (3) are evaluated only once.

B. Extraction of Singularity

$G(u, v, w)$ is singular at $(u, v, w) = (2ma, 2nb, 2pc)$ for $m, n, p = 0, 1, 2, \ldots$. Those singularities that fall into the range of approximation must be removed before any modeling by polynomials is carried out. Since the source and observation points are allowed to be anywhere inside the box, (3) indicates that we only need to consider $\{0 \le u \le 2a, 0 \le v \le 2b, 0 \le w \le 2c\}$ for polynomial modeling because $G(u, v, w)$ is an even function. There are only eight singular points on the corners of the above region in (u, v, w) space, which must be subtracted. These simple terms will be added back to the final polynomial model when the Green's function is used in an SIE–MoM formulation. Any singular term in (4a) can be written in the following form after subtracting its singular part:

$$\frac{e^{-jkR}}{R} = \left(\frac{e^{-jkR}}{R} - \frac{1}{R}\right) + \frac{1}{R} \tag{6}$$

where $R = R_{mnp}$ vanishes within the approximation region. The remaining term in parentheses is continuous at $R = 0$, but its derivative is discontinuous at this point, i.e., it is not an entirely smooth function. Since the convergence of the Chebyshev

polynomial series will suffer significantly from the above discontinuity, a second term is extracted to remove the singularity in the first derivative as follows:

$$\frac{e^{-jkR}}{R} = \left(\frac{e^{-jkR}}{R} - \frac{1}{R} + \frac{k^2}{2}R\right) + \frac{1}{R} - \frac{k^2}{2}R. \quad (7)$$

Similar terms are subtracted from all singular terms corresponding to $m, n, p = \{0, 1\}$ in (4a). Finally, the following function will be approximated by a series of Chebyshev polynomials:

$$\widetilde{G}(u, v, w) = G(u, v, w) - \frac{1}{4\pi} \sum_{m,n,p=0}^{1} \left(\frac{1}{R_{mnp}} - \frac{k^2}{2}R_{mnp}\right). \quad (8)$$

Note that $\widetilde{G}(u, v, w)$ is no longer an even function, but it is still symmetric with respect to $u = a$, $v = b$, and $w = c$ planes

$$\widetilde{G}(u, v, w) = \widetilde{G}(2a - u, 2b - v, 2c - w). \quad (9)$$

C. Best Polynomial Approximation

Approximation of functions of several variables known as *best polynomial product approximation* or *product Chebyshev approximation* have been studied by numerous authors [10], [11]. In this paper, starting from the orthogonality of Chebyshev polynomials, it is shown that the best polynomial approximation of a multivariate function can be easily obtained through FCT. $\widetilde{G}(u, v, w)$ in (8) is approximated by a series of Chebyshev polynomial products in the following form:

$$\widetilde{G}(u, v, w) \approx \tilde{\Phi}(\tilde{u}, \tilde{v}, \tilde{w}) \triangleq \sum_{i=0}^{2I} \sum_{j=0}^{2J} \sum_{k=0}^{2K} \gamma_{ijk} T_i(\tilde{u}) T_j(\tilde{v}) T_k(\tilde{w}) \quad (10)$$

where $T_m(x)$ is the Chebyshev polynomial of order m and $\tilde{u}$, $\tilde{v}$, and $\tilde{w}$ are

$$\tilde{u} = \frac{u}{a} - 1 \quad \tilde{v} = \frac{v}{b} - 1 \quad \tilde{w} = \frac{w}{c} - 1. \quad (11)$$

Normalized variables defined in (11) are limited to $[-1, 1]$, which is the proper range for Chebyshev polynomials over which they are orthogonal. Using (9), it can be shown that $\tilde{\Phi}(\tilde{u}, \tilde{v}, \tilde{w})$ is a symmetric function over $[-1, 1]$ with respect to all three normalized variables. Therefore, in (10), all the odd-order coefficients are zero and the series contains only polynomials of even order

$$\tilde{\Phi}(\tilde{u}, \tilde{v}, \tilde{w}) = \sum_{i=0}^{I} \sum_{j=0}^{J} \sum_{k=0}^{K} \beta_{ijk} T_{2i}(\tilde{u}) T_{2j}(\tilde{v}) T_{2k}(\tilde{w}). \quad (12)$$

For an approximation of order $2I \times 2J \times 2K$, there are only $(I + 1) \times (J + 1) \times (K + 1)$ coefficients. They are obtained after using the orthogonality of the Chebyshev polynomials over $[-1, 1]$ as follows:

$$\beta_{ijk} = \frac{8\delta_i\delta_j\delta_k}{\pi^3} \times \int\int\int_{-1}^{+1} \tilde{\Phi}(\tilde{u}, \tilde{v}, \tilde{w}) \frac{T_{2i}(\tilde{u})}{\sqrt{1 - \tilde{u}^2}} \times \frac{T_{2j}(\tilde{v})}{\sqrt{1 - \tilde{v}^2}} \frac{T_{2k}(\tilde{w})}{\sqrt{1 - \tilde{w}^2}} d\tilde{u} d\tilde{v} d\tilde{w} \quad (13)$$

in which $\delta_i = (1/2)$ when $i = 0$ and $\delta_i = 1$ when $i \neq 0$. After changing the variables to $\tilde{u} = \cos\alpha$, $\tilde{v} = \cos\xi$, and $\tilde{w} = \cos\zeta$, (13) takes the following form:

$$\beta_{ijk} = \frac{8\delta_i\delta_j\delta_k}{\pi^3} \times \int\int\int_{0}^{\pi} \tilde{G}\left(a(1 + \cos\alpha), b(1 + \cos\xi), c(1 + \cos\zeta)\right) \times \cos(2i\alpha)\cos(2j\xi)\cos(2k\zeta) d\alpha d\xi d\zeta \quad (14)$$

for $i = 0, 1, \ldots, I$, $j = 0, 1, \ldots, J$, and $k = 0, 1, \ldots, K$. For each of the integration variables, the integrand in (14) is an analytic function in $[0, \pi]$, which is also periodic with a period of π. The trapezoidal quadrature rule is well known in achieving spectral accuracy for such integrands. Using a trapezoidal rule for numerical integration, (14) is reduced to

$$\beta_{ijk} = \frac{8\delta_i\delta_j\delta_k}{MNP} \sum_{m=0}^{M} \sum_{n=0}^{N} \sum_{p=0}^{P} \epsilon_m\epsilon_n\epsilon_p \widetilde{G}_{mnp} \times \cos\left(2i\frac{m\pi}{M}\right)\cos\left(2j\frac{n\pi}{N}\right)\cos\left(2k\frac{p\pi}{P}\right) \quad (15a)$$

$$\widetilde{G}_{mnp} = \widetilde{G}\left(a\left(1 + \cos\frac{m\pi}{M}\right), b\left(1 + \cos\frac{n\pi}{N}\right), c\left(1 + \cos\frac{p\pi}{P}\right)\right) \quad (15b)$$

$$\epsilon_m = \begin{cases} \frac{1}{2}, & m = 0, M \\ 1, & m = 1, 2, \ldots, M - 1. \end{cases} \quad (15c)$$

Equation (15a) is a three-dimensional (3-D) discrete cosine transform of $\widetilde{G}_{mnp}$. M, N, and P are one less than the number of samples along each of the normalized coordinates and they must be an integer power of two in order to use the fastest FCT algorithm. Equation (15a) is numerically implemented using three levels of one-dimensional (1-D) FCTs corresponding to each of the summations. At each level, a number of 1-D FCTs are performed in parallel on different rows of a 3-D matrix of data. After each level of transforms is completed, only the elements of even order in the resulting sequence are retained. Odd-order elements are all zero and will be discarded so that no unnecessary FCTs are performed in the next level.

An interesting property of product Chebyshev approximation is that the series can be simply truncated to obtain the best approximation of the original function over a lower order manifold of orthogonal polynomials. Therefore, if the order of approximating a polynomial along the $\tilde{u}$ dimension is chosen to be $2I$, the sequence obtained from FCT in this direction will be truncated at $2I + 1$, and after its odd-order elements are removed, only $I + 1$ elements, instead of the entire $M/2 + 1$ terms, will be restored. Similar truncation takes place in the other two directions. In practice, it was observed that usually $M = N = P = 2^5$ is more than enough for accurate sampling of the Green's function in conductor loaded resonators and $4 \leq I = J = K \leq 6$ leads to a highly accurate polynomial model in these applications.

For each pair of arbitrary source and observation points, the series in (12) is evaluated through an algorithm due to Clenshaw [12], [13] specialized for Chebyshev polynomial series. This algorithm takes advantage of the recurrence relations between Chebyshev functions and involves a minimum number of mathematical operations. Another interesting property of Chebyshev polynomials is the following identity:

$$T_{2i}(\tilde{u}) = T_i\big(2\tilde{u}^2 - 1\big). \tag{16}$$

The above identity means that mathematical complexity of an even series made of $T_0(\tilde{u}), T_2(\tilde{u}), T_4(\tilde{u}), \ldots, T_{2I}(\tilde{u})$ is equal to the complexity of the series that only contains $T_0(\tilde{u}), T_1(\tilde{u}), T_2(\tilde{u}), \ldots, T_I(\tilde{u})$ and the computational time is further reduced by a factor of two.

D. Sampling the Green's Function

The Ewald sum technique is employed to evaluate the samples of the Green's function required for polynomial modeling. These samples are given by (15b) and the Ewald method is applied to (4a) to calculate (8) as quickly as possible. Final expressions for (4a) after applying the Ewald transform are the following:

$$G = G_1 + G_2 \tag{17a}$$

$$G_1 = \frac{1}{abc} \sum_{m,n,p=0}^{+\infty} \frac{\delta_m \delta_n \delta_p}{\alpha_{mnp}^2} \times e^{-\frac{\alpha_{mnp}^2}{4E^2}} \cos\frac{m\pi u}{a} \cos\frac{n\pi v}{b} \times \cos\frac{p\pi w}{c} \tag{17b}$$

$$G_2 = \frac{1}{4\pi} \sum_{m,n,p=-\infty}^{+\infty} \frac{\Re\left[e^{-jkR_{mnp}} \operatorname{erfc}\left(R_{mnp}E - \frac{jk}{2E}\right)\right]}{R_{mnp}} \tag{17c}$$

$$\alpha_{mnp}^2 = \left(\frac{m\pi}{a}\right)^2 + \left(\frac{n\pi}{b}\right)^2 + \left(\frac{p\pi}{c}\right)^2 - \epsilon_r k_o^2. \tag{17d}$$

E is the splitting parameter in the Ewald method and a good estimate for its optimum value is found in [14]. A number of practical issues in numerical implementation of the above expressions were addressed by the authors in [8]. They include an expression for the residue after extracting the singularity, as required by (8), and replacement of the complex error function with a special real valued quadrature formula, which further enhances the speed of calculations. Using the Ewald method enables the polynomial modeling to be very fast so that its computational time at each frequency is negligible compared to the time required for the matrix filling in MoM.

III. SIE–MoM Formulation

In order to verify the efficiency and accuracy of the product polynomial model for the Green's function developed in Section II, it is used in an SIE formulation to find the resonant frequencies of some conductor loaded cavity resonators. Two types of resonators are considered: a cavity loaded with a metallic disc, as shown in Fig. 2, and a combline cavity resonator, as shown in Fig. 3.

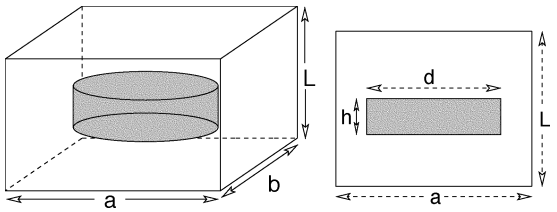

Fig. 2. Cavity loaded with a perfectly conducting disk.

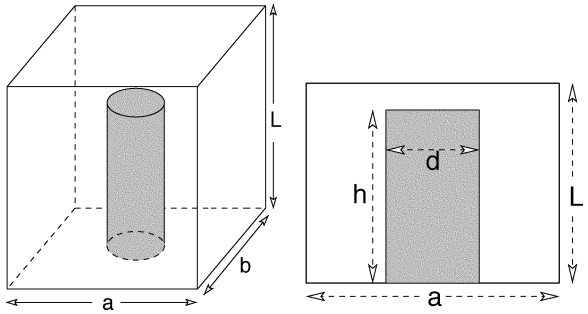

Fig. 3. Combline resonator.

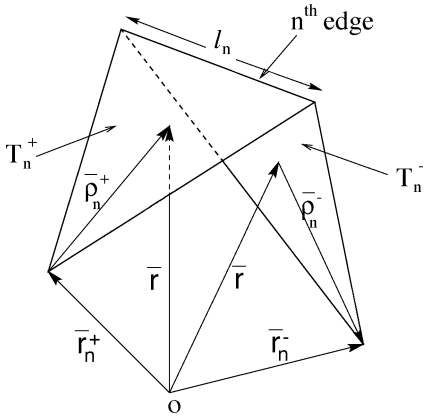

Fig. 4. RWG basis function $\vec{f}_n(\vec{r})$.

An electric-field mixed potential integral equation (MPIE) is employed, which is well known for its more stable and robust solution with less singular kernel. The surface current on the metallic object inside the cavity is expanded in terms of well-known RWG basis functions [15], shown in Fig. 4, as follows:

$$\vec{J}_s = \sum_{n=0}^{N-1} I_n \vec{f}_n(\vec{r}). \tag{18}$$

Since the cavity is closed and there is no excitation field, the tangential component of the electric field generated by the above current must be zero over the surface of the conductor inside cavity

$$-\vec{E}_{\tan}(\vec{J}_s) = \Big(j\omega\mu\vec{A}(\vec{J}_s) + \nabla\phi(\rho_s)\Big)_{\tan} = 0. \tag{19}$$

$\rho_s = -(1)/(j\omega)\nabla_s \cdot \vec{J}_s$ is the surface charge density and $\vec{A}$ and ϕ are the magnetic vector potential and scalar electric potential, respectively. Following the Galerkin procedure for solving the

integral equation, (19) is tested by the same RWG basis functions and the final expressions for the MoM matrix elements are obtained as follows:

$$\sum_{n=0}^{N-1} I_n \left\{ a_{mn} - \frac{1}{k^2} q_{mn} \right\} = 0, \qquad m = 0,1,2,\ldots,N-1 \tag{20a}$$

$$a_{mn} = \int_{S_m} \vec{f}_m(\vec{r}) \cdot \int_{S_n} \bar{\bar{G}}_A(\vec{r},\vec{r}') \cdot \vec{f}_n(\vec{r}')ds'ds \tag{20b}$$

$$q_{mn} = \int_{S_m} \nabla_s \cdot \vec{f}_m(\vec{r}) \int_{S_n} G_q^e(\vec{r},\vec{r}')\nabla_s' \cdot \vec{f}_n(\vec{r}')ds'ds. \tag{20c}$$

S_m is the area of the mth basis function, which consists of two triangles [15]. Note that (20a) leads to an eigenvalue problem from which the resonant frequency is found by looking at the eigenvalue of the coefficient matrix that has the lowest magnitude. At resonance, this eigenvalue will become zero and the corresponding eigenvector is proportional to the modal surface current on the resonator. It is worth mentioning that the matrix of coefficients in (20a) is real valued and symmetric, which reduces the time for eigenvalue computations considerably.

In order to evaluate the efficiency of the new method for Green's function calculations, both the Ewald sum technique [8] and Chebyshev polynomial model are used in the MoM formulation. In both cases, the singularity of the Green's function must be extracted when the source and observation triangles coincide. As stated in Section II-B, the Green's function shows a discontinuous derivative even after the $1/R$ singularity is extracted. Therefore, similar to (7), another term is also extracted to remove the singularity in the first derivative before any numerical integration. As a result, (20b) and (20c) will take the following form:

$$a_{mn} = \int_{S_m} \vec{f}_m \cdot \int_{S_n} \left(\bar{\bar{G}}_A - \sigma S \bar{\bar{I}} \right) \cdot \vec{f}_n ds'ds + \sigma \int_{S_m} \vec{f}_m \cdot \int_{S_n} S(\vec{r},\vec{r}')\vec{f}_n ds'ds \tag{21a}$$

$$q_{mn} = \int_{S_m} \nabla_s \cdot \vec{f}_m \int_{S_n} \left(G_q^e - \sigma S \right) \nabla_s' \cdot \vec{f}_n ds'ds + \sigma \int_{S_m} \nabla_s \cdot \vec{f}_m \int_{S_n} S(\vec{r},\vec{r}')\nabla_s' \cdot \vec{f}_n ds'ds \tag{21b}$$

$$S = \frac{1}{4\pi} \left(\frac{1}{|\vec{r}-\vec{r}'|} - \frac{k^2}{2}|\vec{r}-\vec{r}'| \right). \tag{21c}$$

σ is used to turn the singularity extraction "on" and "off" according to the relative locations of the source and observation triangles, i.e., $\sigma = 1$, when the source and observation triangles overlap, and $\sigma = 0$ when the two triangles are separate. The first terms in (21a) and (21b) are easily integrated using quadrature formulas specialized for triangular domains [16], [17]. Decomposition of integrals, as shown in (21), helps to reduce the matrix filling time significantly because the smooth kernels allow us to use low-order quadrature rules with no loss of accuracy. Only a three-point quadrature was used to calculate each of the integrals. Inner integrals of $S(\vec{r},\vec{r}')$ in (21c) are carried out analytically using formulas given in [18] and [19], and the outer integrals are calculated numerically using the same quadrature rules.

TABLE I
COMPARISON BETWEEN THE EWALD METHOD AND THE NEW SCHEME

ϵ_r	I, J, K	Ewald time	polynomial time	max. error	Chebyshev approx.
1	4, 4, 4	16.73 sec	0.66 sec	1.241×10^{-5}	1.19 sec
10	6, 5, 5	23.77 sec	1.03 sec	1.607×10^{-4}	1.42 sec
20	8, 7, 7	25.01 sec	1.44 sec	8.541×10^{-5}	1.57 sec

IV. NUMERICAL RESULTS

Numerical experiments were carried out on an AMD Athlon XP processor with 2.2-GHz clock frequency. All programs are written in C++ and compiled with a GNU C++ compiler.

A. Green's Function Calculations

To compare the accuracy and computational speed of the new polynomial model with that of the Ewald sum technique, potential Green's functions were calculated at 80 000 points inside a rectangular cavity using both methods. Dimensions of the cavity are $a = 45$ mm, $b = 40$ mm, and $c = 35$ mm, and the source is located at $x' = 22.5$ mm, $y' = 20$ mm, and $z' = 17.5$ mm. Observation points are chosen over two grids of 200×200 points on $z = z'$ and $z = 20$ planes. Frequency is fixed at 2.0 GHz and the cavity is uniformly filled with a homogeneous material with a dielectric constant of ϵ_r. The results are reported in Table I. The calculated error is the maximum relative difference between the Chebyshev series model and the Ewald method over the entire 80 000 points for all components of $\bar{\bar{G}}_A$. Polynomials of higher degrees are needed to keep the maximum error at an acceptable level when the dielectric constant of the material inside the box is increased. Note that the new scheme is up to 20 times faster than the Ewald method and, with a higher level of acceptable error, the new scheme can be made even faster. In all cases, 32 sample points were taken in each of the three spatial directions $(M = N = P = 32)$. Reducing the number of samples down to 20 would not make any difference in accuracy of the final polynomial series, but the time required for Chebyshev modeling is at its minimum when the number of samples is an integer power of two. At lower frequencies or low dielectric constants, one can choose 16 samples in each direction with no loss of accuracy and highest computational speed.

A 3-D plot of G_A^{xx} is shown in Fig. 5, in which only the first term of (21c) is subtracted [similar to (6)]. The discontinuity in the first derivative is evident at the center of the plot where the source is located. This effect is more profound at higher frequencies or higher dielectric constants. In Fig. 6, both terms of (21c) are subtracted and the Green's function is smooth enough to be integrated with a low-order quadrature with high accuracy.

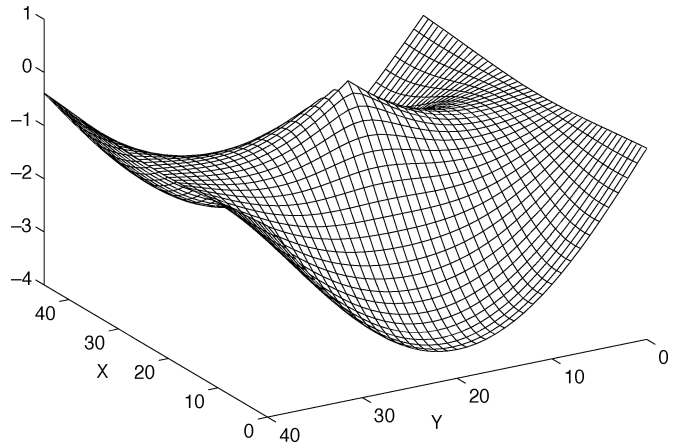

Fig. 5. 3-D plot of $(G_A^{xx})/(\mu_0) - (1)/(4\pi R)$.

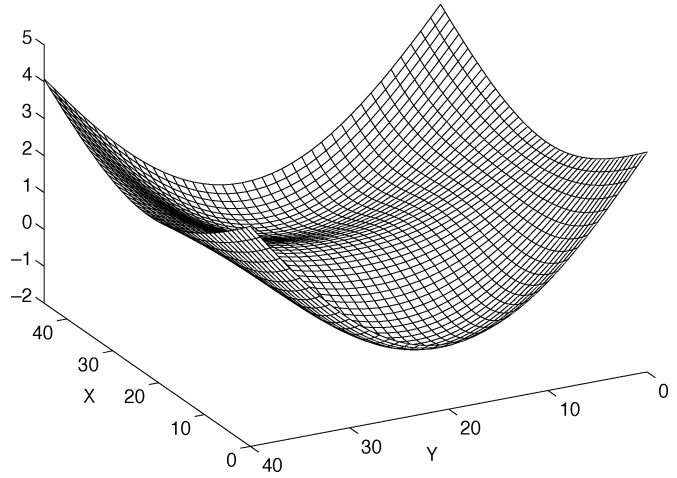

Fig. 6. 3-D plot of $(G_A^{xx})/(\mu_0) - (1/4\pi)((1/R - k^2/2)R)$.

TABLE II
RESULTS FOR DISK-LOADED CAVITY

resonant frequency: HFSS	4111.4MHz, 4199.8MHz
resonant frequency: SIE-MoM	4110.66MHz, 4198.89MHz
matrix filling: Chebyshev series	12.3 sec
matrix filling: Ewald method	334.15 sec
Chebyshev approximation	1.3 sec

B. Resonant Frequencies and SIE MoM

As stated in Section III, an SIE with a Galerkin method was employed to calculate the resonant frequency of two types of conductor loaded resonators shown in Fig. 2 and Fig. 3. To verify the results obtained from the integral-equation technique, the resonant frequencies are also computed via the High Frequency Structure Simulator (HFSS), a well-known commercial software from the Ansoft Corporation. For the combline resonator, measured results from [20] are also included.

In Table II, the first two resonant frequencies of a disk-loaded cavity resonator are reported. Referring to Fig. 2, dimensions of the structure are $a = 36$ mm, $b = 35$ mm, $L = 30$ mm, $d = 24$ mm, and $h = 6$ mm, and the disk is located at the center of the cavity. Both the Ewald transform and new

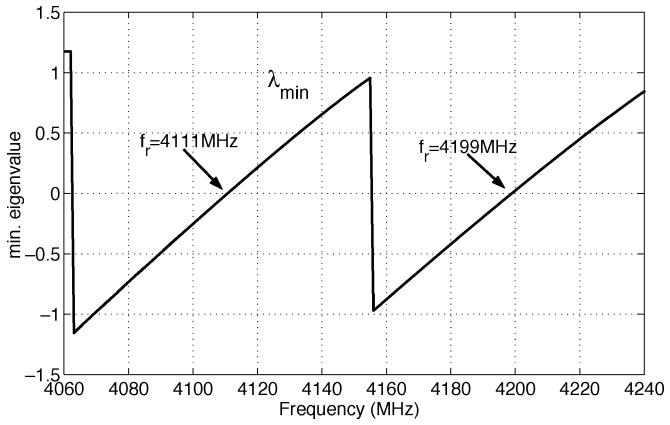

Fig. 7. Smallest eigenvalue of the MoM matrix for a disk resonator.

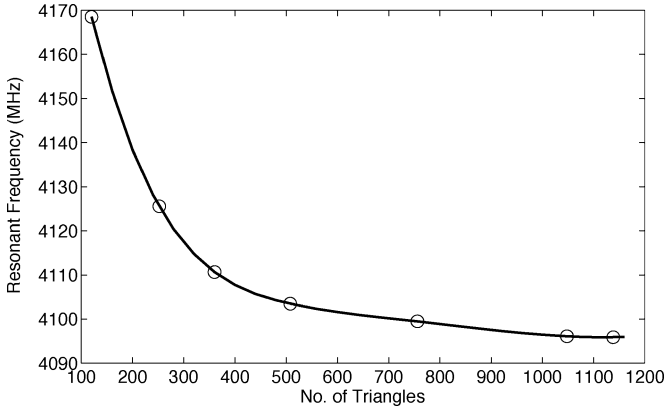

Fig. 8. Convergence of the MoM versus the number of triangular elements.

Chebyshev series model for Green's functions were used and the CPU time required to fill the entire MoM matrix are compared. The perimeter of the disk was divided into $N_\phi = 24$ segments both in SIE–MoM formulation and HFSS. After mesh generation, the surface of the metallic disk was divided into 360 triangles, leading to 540 RWG basis functions. In this test, the symmetry of the coefficient matrix was not exploited and the entire 540 $\times$ 540 elements were calculated directly. Resonant frequency was obtained by looking at the smallest eigenvalue of the MoM matrix, which is plotted in Fig. 7 versus frequency. It is evident that the resonant frequencies obtained from the SIE–MoM approach are highly accurate and the computational efficiency of the new scheme is greatly enhanced compared to that of the Ewald sum technique.

Convergence of the MoM in finding the resonant frequency versus the number of triangular elements was also investigated, and the results are shown in Fig. 8 and Table III. N_ϕ is the number of segments on the perimeter of the disk and N_z is the number of segments along the thickness.

The sequence of coefficients for polynomial approximation obtained from the FCT algorithm are in descending order and, as stated in Section II-C, the series is truncated when the corresponding coefficient is less than a prescribed error tolerance. Table IV shows the resonant frequencies obtained for different tolerances by which the Chebyshev series are truncated. Higher tolerance leads to lower order polynomials. The time reported in Table III and Table IV is the total time for each frequency

TABLE III
CONVERGENCE OF THE MOM VERSUS NUMBER OF BASIS FUNCTIONS

segmentation	f_r MHz	Triangles	RWG	time/iter
$N_\phi = 12\ N_z = 3$	4168.5	120	180	2.8 sec
$N_\phi = 18\ N_z = 3$	4125.5	252	378	6.2 sec
$N_\phi = 24\ N_z = 3$	4110.6	360	540	11.5 sec
$N_\phi = 30\ N_z = 3$	4103.5	508	762	21.6 sec
$N_\phi = 36\ N_z = 3$	4099.5	756	1134	47 sec
$N_\phi = 45\ N_z = 3$	4096.1	1048	1572	91 sec
$N_\phi = 45\ N_z = 4$	4095.8	1138	1707	107 sec

TABLE IV
EFFECT OF ACCURACY IN CHEBYSHEV APPROXIMATION ON RESONANT FREQUENCY

f_r MHz	I, J, K	tolerance	time/iter
4110.7	6, 6, 5	10^{-6}	18.7 sec
4110.7	5, 5, 4	10^{-5}	13.8 sec
4110.6	5, 4, 3	10^{-4}	11.5 sec
4111.4	4, 3, 2	10^{-3}	8.7 sec
4107.9	3, 2, 2	10^{-2}	7.5 sec
4145.4	2, 1, 1	10^{-1}	6.0 sec

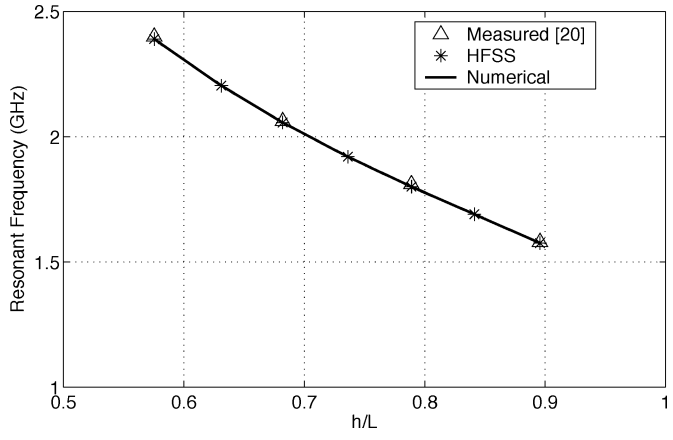

Fig. 9. Computed and measured results for the resonant frequency of the combline resonator. Measured results are from [20].

step, including the Chebyshev approximation, matrix filling, and finding the eigenvalue of the matrix.

As a second example, the resonant frequency of a combline cavity, shown in Fig. 3, was computed. The physical dimensions are $a = 1$ in, $b = 0.872$ in, $L = 1.872$ in, and $d = 0.26$ in. For mesh generation, the perimeter of the metallic post was divided into $N_\phi = 18$ segments with $N_z = 10$ divisions along its height. A triangular mesh with 432 elements was generated leading to 657 RWG basis functions. Resonant frequency of the dominant mode for different lengths of the conducting post is plotted in Fig. 9 along with the results from HFSS simulation and measurements from [20]. Matrix filling takes only 12.4 s at each frequency compared to 344 s when using the Ewald transform.

V. CONCLUSION

A novel scheme for fast computation of the Green's functions in a rectangular cavity has been presented. The method is based on a Chebyshev polynomial series approximation of the Green's function, which is carried out using an FCT in 3-D. Samples of the Green's function required for the approximation are generated via the Ewald sum method.

Resonant frequency of two conductor loaded cavity resonators were obtained using a mixed-potential SIE formulation in which the cavity Green's functions were employed. Using the new scheme for computing the Green's functions leads to a significant reduction in computation times compared to the Ewald summation technique. A number of practical issues in numerical implementation of the MoM were addressed, which further enhance the numerical efficiency and stability of the method.

The new approach is considered to be a major step toward practical application of integral-equation techniques for electromagnetic analysis of arbitrary shape objects inside rectangular cavities. In particular, novel structures including dielectric or metallic resonators featuring cuts and round corners can be investigated and optimized within a reasonable computational time.

REFERENCES

[1] W. Wallyn, D. De Zutter, and H. Rogier, "Prediction of the shielding and resonant behavior of multisection enclosures based on magnetic current modeling," *IEEE Trans. Electromagn. Compat.*, vol. 44, pp. 130–138, Feb. 2002.

[2] J.-F. Liang, H.-C. Chang, and K. A. Zaki, "Coaxial probe modeling in waveguides and cavities," *IEEE Trans. Microwave Theory Tech.*, vol. 40, pp. 2172–2180, Dec. 1992.

[3] M. S. Leong, L. W. Li, P. S. Kooi, T. S. Yeo, and S. L. Ho, "Input impedance of a coaxial probe located inside a rectangular cavity: Theory and experiment," *IEEE Trans. Microwave Theory Tech.*, vol. 44, pp. 1161–1164, July 1996.

[4] J. M. Jarem, "A multifilament method-of-moments solution for the input impedance of a probe-excited semi-infinite waveguide," *IEEE Trans. Microwave Theory Tech.*, vol. MTT-35, pp. 14–19, Jan. 1987.

[5] K. E. Jordan, G. R. Richter, and P. Sheng, "An efficient numerical evaluation of the Green's function for the Helmholtz operator on periodic structures," *J. Comput. Phys.*, vol. 63, pp. 222–235, 1986.

[6] M. J. Park, J. Park, and S. Nam, "Efficient calculation of the Green's function for the rectangular cavity," *IEEE Microwave Guided Wave Lett.*, vol. 8, pp. 124–126, Mar. 1998.

[7] F. Marliani and A. Ciccolella, "Computationally efficient expressions of the Dyadic Green's function for rectangular enclosures," *Progress in Electromagn. Res.*, vol. 31, pp. 195–223, 2001.

[8] A. Borji and S. Safavi-Naeini, "Fast convergent Green's function in a rectangular enclosure," in *IEEE AP-S Int. Symp.*, vol. 4, Columbus, OH, 2003, pp. 950–953.

[9] M. Bressan, L. Perregrini, and E. Regini, "BI-RME modeling of 3D waveguide components enhanced by the Ewald technique," in *IEEE MTT-S Int. Microwave Symp. Dig.*, vol. 2, 2000, pp. 1097–1100.

[10] S. E. Weinstein, "Approximations of functions of several variables: Product Chebyshev approximations I," *J. Approx. Theory*, vol. 2, pp. 433–447, 1969.

[11] J. N. Henry, M. S. Henry, and D. Schmidt, "Numerical comparisons of algorithms for polynomial and rational multivariable approximations," *SIAM J. Numer. Anal.*, vol. 15, no. 6, pp. 1197–1207, Dec. 1978.

[12] C. W. Clenshaw, *Mathematical Tables: Chebyshev Series for Mathematical Functions*. London, U.K.: Nat. Phys. Lab., 1962, vol. 5.

[13] W. H. Press, S. A. Teukolsky, W. T. Vetterling, and B. P. Flannery, *Numerical Recipes in C*, 2nd ed. Cambridge, U.K.: Cambridge Univ. Press, 1992, sec. 5.8–5.10.

[14] A. Kustepeli and A. Q. Martin, "On the splitting parameter in the Ewald method," *IEEE Microwave Guided Wave Lett.*, vol. 10, pp. 168–170, May 2000.

[15] S. M. Rao, D. R. Wilton, and A. W. Glisson, "Electromagnetic scattering by surfaces of arbitrary shape," *IEEE Trans. Antennas Propagat.*, vol. AP-30, pp. 409–417, May 1982.

[16] G. R. Cowper, "Gaussian quadrature formulas for triangles," *Int. J. Numer. Methods Eng.*, vol. 7, pp. 405–408, 1973.
[17] D. A. Dunavant, "High degree efficient symmetrical Gaussian quadrature rules for the triangle," *Int. J. Numer. Methods Eng.*, vol. 21, pp. 1129–1148, 1985.
[18] P. Yla-Oijala and M. Taskinen, "Calculation of CFIE impedance matrix elements with RWG and $n \times \mathrm{RWG}$ functions," *IEEE Trans. Antennas Propagat.*, vol. 51, pp. 1837–1846, Aug. 2003.
[19] R. D. Graglia, "On the numerical integration of the linear shape functions times the 3-D Green's function or its gradient on a plane triangle," *IEEE Trans. Antennas Propagat.*, vol. 41, pp. 1448–1455, Oct. 1993.
[20] H. W. Yao, K. A. Zaki, A. E. Atia, and R. Hershtig, "Full wave modeling of conducting posts in rectangular waveguides and its applications to slot coupled combline filters," *IEEE Trans. Microwave Theory Tech.*, vol. 43, pp. 2824–2829, Dec. 1995.

Amir Borji (S'99–M'04) was born in Tehran, Iran, in August 1971. He received the B.Sc. and M.Sc. degrees in electrical engineering from the Isfahan University of Technology, Isfahan, Iran, in 1994 and 1998, respectively, and the Ph.D. degree in electrical engineering from University of Waterloo, Waterloo, ON, Canada in 2004.

He is currently a Post-Doctoral Fellow with the Department of Electrical and Computer Engineering, University of Waterloo. His research interests include synthesis, design, and optimization of various microwave filters and full-wave electromagnetic analysis of shielded structures using integral-equation methods.

Dr. Borji was the recipient of the 2002 Ontario Graduate Scholarship Award.

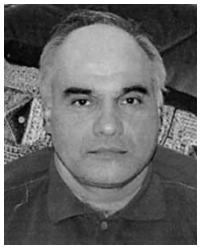

Safieddin Safavi-Naeini (S'75–M'78) received the B.Sc. degree in electrical engineering from the University of Tehran, Tehran, Iran, in 1974, and the M.Sc. and Ph.D. degrees in electrical engineering from the University of Illinois at Champaign-Urbana, in 1975 and 1979, respectively.

From 1980 to 1995, he was an Assistant Professor and then an Associate Professor with the Electrical Engineering Department, University of Tehran. In 1996, he joined the University of Waterloo, Waterloo, ON, Canada, where he is currently a Professor with the Department of Electrical and Computer Engineering. He has been a scientific and technical consultant to numerous national and international telecom industrial and research organizations over the last 20 years. He has authored or coauthored over 130 papers in technical journals and conferences. His research interests and activities include numerical electromagnetics applied to analysis and design optimization of RF/microwave/millimeter-wave systems and circuits, antenna and propagation, wireless communication systems, very high-speed digital circuits, and photonics.